

Lattice QCD : Flavor Physics and Spectroscopy

Takashi Kaneko*

*High Energy Accelerator Research Organization (KEK), Ibaraki 305-0801, Japan
School of High Energy Accelerator Science, SOKENDAI (The Graduate University for Advanced
Studies), Ibaraki 305-0801, Japan*

**E-mail: takashi.kaneko@kek.jp*

We review highlights of recent results on the hadron spectrum and flavor physics from lattice QCD. We also discuss recent rapid progress on the muon anomalous magnetic moment.

Keywords: Style file; L^AT_EX; Proceedings; World Scientific Publishing.

1. Introduction

Lattice QCD plays a key role in the intensity frontier to search for new physics. Interpretation of experimental measurements within and beyond the Standard Model (SM) requires precise knowledge on the relevant hadronic matrix elements, which describe nonperturbative QCD effects in the underlying processes. Moreover, high statistics data produced at flavor factories brought rich outcome about the hadron spectrum, such as the discoveries of exotic hadrons. Nonperturbative dynamics of QCD characterizes their properties which do not fit into the simple quark model prediction. Lattice QCD is the only known method for ab initio studies of these nonperturbative aspects with systematically improvable uncertainties.

Lattice QCD is a regularization of QCD on a discrete Euclidean space-time lattice. In finite volume, the QCD path integral is reduced into a finite-dimensional integral and can be numerically evaluated by Monte Carlo sampling of gauge field configurations on a computer. Pioneering simulations had been limited to small and coarse lattices with unphysically heavy and degenerate up and down quarks. Such limitations have been gradually lifted by advances in computing power and continuous development of lattice QCD formulations and simulation algorithms. We note that the lattice formulation is not unique: the action has a degree of freedom to add irrelevant terms, which vanish in the limit of zero lattice spacing $a \rightarrow 0$, namely the continuum limit. We can exploit this freedom to improve properties of the lattice action and to firmly establish lattice predictions by independent calculations with different actions.

Lattice simulations can straightforwardly study the spectrum and transition amplitude of hadrons which are stable under QCD. The light hadron spectrum, for instance, has been reproduced by simulations on fine and large lattices with light quark masses close to their physical values¹⁻⁴. While implementation of QED is not straightforward on a finite periodic space-time volume⁵, even the permille-level

neutron–proton mass splitting is now reproduced by taking account of electromagnetic (EM) effects and strong isospin breaking due to the up and down quark mass splitting $m_u - m_d$ ^{6,7}. The accuracy of simple kaon matrix elements, namely the decay constant, form factors and bag parameters, also attains the percent level or better. Such precision lattice calculation is now being extended to heavy-flavored hadrons, which offer rich probes of new physics.

The study of hadronic decays, however, meets technical difficulties. As suggested by Maiani–Testa theorem⁸, there is no simple relation between the strong decay amplitudes and correlation functions on the Euclidean lattice. Theoretical frameworks are under active development in order to study the $K \rightarrow \pi\pi$ decay as well as the heavy quarkonia and exotic states, which generally lie above thresholds.

In this article, we review highlights of recent lattice studies on the hadron spectrum and flavor physics. We also briefly discuss recent rapid progress on the muon anomalous magnetic moment, which is a key quantity in the search of new physics. More detailed reviews on these topics can be found in Refs. 9–13.

2. Hadron spectroscopy

If a hadron H is stable under QCD, it is straightforward to calculate its energy E_H on the lattice. We prepare an interpolating field \mathcal{O}_H with quantum numbers of H , and extract E_H from the asymptotic behavior of the two-point function towards the large Euclidean temporal separation $t \rightarrow \infty$

$$\langle \mathcal{O}_H(t) \mathcal{O}_H^\dagger(0) \rangle \rightarrow \frac{|Z_H|^2}{2E_H} e^{-E_H t}. \quad (1)$$

Here $Z_H = \langle 0 | \mathcal{O}_H | H \rangle$ represents the overlap of \mathcal{O}_H with the physical state $|H\rangle$. This simple method forms a basis for the recent predictions for the low-lying hadron spectrum mentioned in Sec. 1.

This can also provide illuminating insight into the nature of yet-unestablished states which are stable under the strong interaction. The doubly charmed baryons Ξ_{cc}^+ and Ξ_{cc}^{++} , for instance, are expected to have large branching fraction to flavor changing decay modes²³. The first observation was reported by the SELEX experiment at $M_{\Xi_{cc}^+} = 3519(2)$ MeV^{24,25} and $M_{\Xi_{cc}^{++}} \sim 3460$ MeV²⁶. This however poses a puzzle of the large isospin splitting $M_{\Xi_{cc}^{++}} - M_{\Xi_{cc}^+} \sim -60$ MeV and short life-times in contrast to phenomenological analyses^{23,27,28}. The left-panel of Fig. 1 is a compilation of recent lattice QCD predictions for the doubly-charmed baryon spectra in the isospin limit^{14–21}. These studies employing different lattice actions have led to reasonable agreement around $M_{\Xi_{cc}} \sim 3600$ MeV, which is systematically higher than the SELEX results but favors recent observation $M_{\Xi_{cc}^{++}} = 3621.40(0.78)$ MeV by LHCb (right panel of Fig. 1). A lattice estimate of the isospin splitting $M_{\Xi_{cc}^{++}} - M_{\Xi_{cc}^+} = 2.2(0.2)$ MeV also contradicts the old measurement.

While studying unstable particles is more involved, there has been considerable progress in recent years. Let us consider a resonance strongly decaying into two

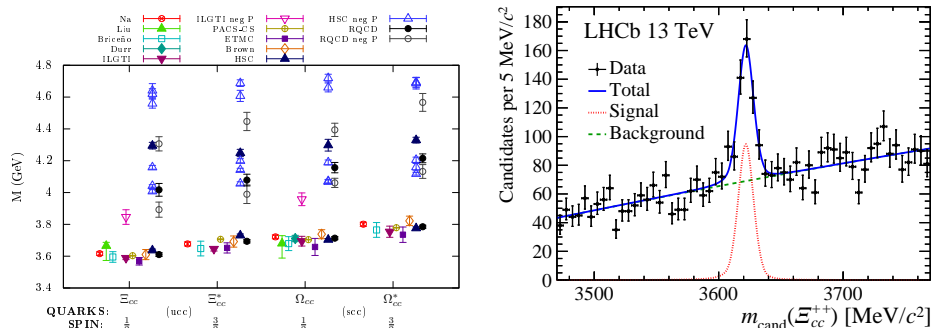


Fig. 1. Left panel: compilation of recent lattice predictions for doubly charmed baryon spectra (figure from Ref. 14). The lowest positive-parity states have been studied by many groups^{14–21}, whereas less results are available for the excited and/or negative-parity states^{14,17,21}. Right panel: invariant mass distribution of $\Xi_{cc}^+ \rightarrow \Lambda_c^+ K^- \pi^+ \pi^+$ decay candidates from LHCb (figure from Ref. 22). pp data sample corrected at a center-of-mass (CM) energy 13 TeV with an integrated luminosity of 1.7 fb^{-1} is analyzed. The dotted, dashed and solid lines are fit curves for the signal, background and their total.

particles A and B . Its mass and width can be determined from the scattering amplitude of A and B , but they are not directly given by the amplitudes of the Euclidean correlation function⁸

$$\langle \mathcal{O}'_{AB}(t) \mathcal{O}_{AB}^\dagger(0) \rangle = \sum_n \frac{Z'_{AB,n} Z_{AB,n}^*}{2E_{AB,n}} e^{-E_{AB,n}t}. \quad (2)$$

Here \mathcal{O}_{AB} and \mathcal{O}'_{AB} represent interpolating fields for the two-particle state AB , and n is the index of the energy levels. However, the spectrum $\{E_{AB,1}, E_{AB,2}, \dots\}$ deviates from the non-interacting energy levels due to the AB scattering on the lattice, and hence encodes the scattering amplitude. Lüscher derived a formula to extract the phase shift from the discrete spectrum on the finite volume^{29–31}. Later the HALQCD Collaboration developed another method to study a multi-particle system^{32–34}. By using an interpolating field $O'_{AB}(t) = O_A(\mathbf{x}, t) O_B(\mathbf{x} + \mathbf{r}, t)$, the HALQCD method extracts the Nambu-Bethe-Salpeter wave function of the two-particle system AB with relative distance $|\mathbf{r}|$, from which the amplitude of the AB scattering can be deduced.

A good application of these methods is rigorous understanding of the resonant $\pi\pi$ and $K\pi$ scatterings directly from QCD. While the original Lüscher formula was limited to a single channel problem for two identical scalar particles in the CM frame, efforts over the past few decades have generalized it to arbitrary two-particle systems also in moving frames^{37–42}. This theoretical development has made rapid stride in the lattice study of the ρ and K^* resonances in the isovector channel^{9,10,43}. The left panel of Fig. 2 shows the scattering phase shift $\delta_1^{\pi\pi(K\pi)}$ obtained by the RQCD Collaboration. They simulate a pion mass $M_\pi \sim 150 \text{ MeV}$ close to its physical value $M_{\pi,\text{phys}}$ in two-flavor QCD³⁵, where only degenerate up and down quarks are

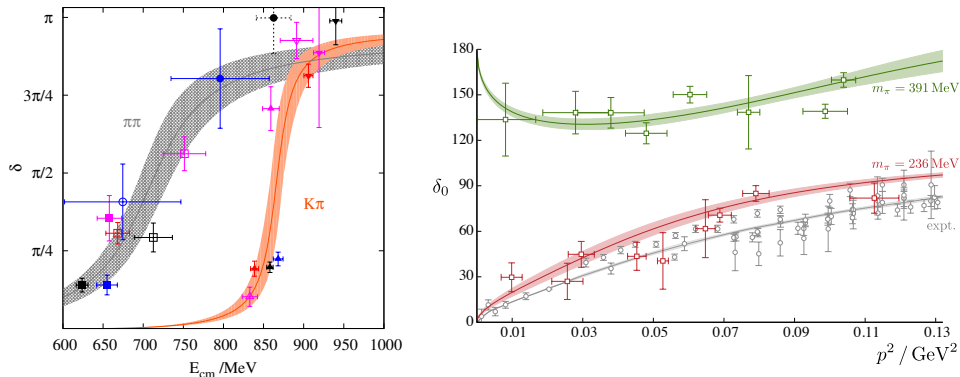


Fig. 2. Left panel: isovector $\pi\pi$ ($\delta_1^{\pi\pi}$, circles and squares) and $K\pi$ ($\delta_1^{K\pi}$, triangles) phase shift against the CM frame energy (figure from Ref. 35). The black shaded and orange bands show the Breit-Wigner parametrization of $\delta_1^{\pi\pi}$ and $\delta_1^{K\pi}$, respectively. Right panel: isoscalar $\pi\pi$ scattering phase shift $\delta_0^{\pi\pi}$ as a function of scattering momentum $p^2 = (E_{\text{CM}}/2)^2 - M_\pi^2$ (figure from Ref. 36).

present in the sea. It is encouraging to observe the rapid raise of $\delta_1^{\pi\pi(K\pi)}$ near the physical ρ (K^*) mass. Although a detailed analysis based on a Breit-Wigner parametrization leads to slight tension in the resonance masses and widths with experiment, it may be attributed to quenching of strange quarks, namely the missing $K\bar{K}$ channel^{44,45}. Calculations in three-flavor QCD, namely with dynamical strange quarks, are being available. For recent studies, see Refs. 46–48 and references therein.

The Lüscher method has been also applied to the isoscalar channel, which is much more challenging than the iso-nonsinglet ones. The relevant two-point function involves the so-called quark-disconnected diagrams (see Fig. 1 of Ref. 36), which are computationally very expensive. The Hadron Spectrum Collaboration have published the first full calculation of the isoscalar scattering phase shift $\delta_0^{\pi\pi}$ ³⁶. It is interesting to observe that σ is a bound state at $M_\pi \sim 390$ MeV, but turns into a broad resonance already at ~ 240 MeV as seen in the right panel of Fig. 2. The mass and width of σ approach their experimental values⁴⁹, as M_π decreases. While a simulation at the physical mass $M_{\pi,\text{phys}}$ is needed to make a direct comparison with experiment, those at unphysical M_π 's deepen our understanding of the existence form of the hadrons: how it changes from unphysical to the real worlds.

Extension to heavy hadrons, particularly exotic hadrons discovered at flavor factories, is intriguing but still challenging task of lattice QCD. These hadrons in general have significant branching fraction to states containing three or more particles. Generalization of Lüscher's framework capable of these high multiplicity states is an active area of lattice QCD^{50–53}. It is not unreasonable to hope that such a general framework will become available in the next decade.

There are however good examples that the current methodology can gain insight into the nature of exotic hadrons. One example is a recent study of $X(5568)$ ⁵⁴. The

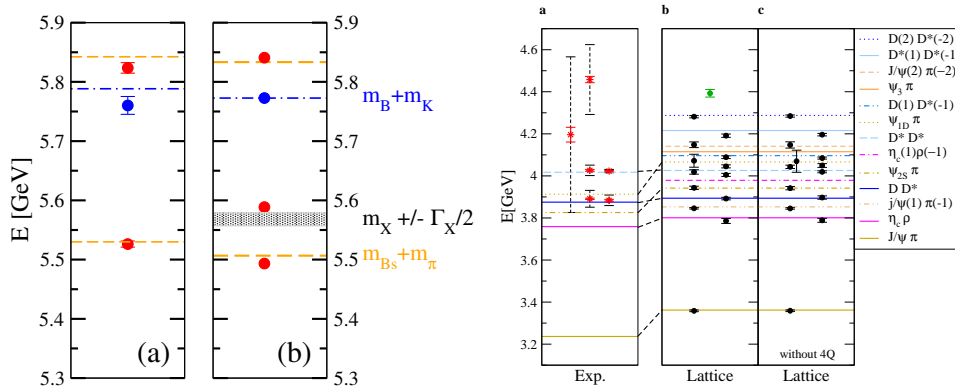


Fig. 3. Left panel: finite volume spectrum for $X(5568)$ (figure from Ref. 54). The sub-panel (a) shows simulation data at $M_\pi \sim 156$ MeV, whereas an analytic prediction at $M_{\pi, \text{phys}}$ is plotted in the sub-panel (b) by assuming the existence of $X(5568)$. The finite volume spectrum ($L = 2.9$ fm) is plotted by circles. The horizontal lines show non-interacting levels of $B_s(0)\pi^+(0)$, $B^+(0)\bar{K}^0(0)$ and $B_s(1)\pi^+(-1)$, where the arguments are lattice momenta in units of $2\pi/L$. Note that the finite volume level (red circle) near the experimental mass (shaded band in sub-panel (b)) is missing in the simulation data (sub-panel (a)). Right panel: finite volume spectrum for $Z_c^+(3900)$ (figure from Ref. 55). The experimental masses of the Z_c candidates discussed in Ref. 56 ($Z_c(3885, 3900, 4020, 4025, 4430)$) are plotted in the sub-panel “a”. The vertical dashed lines represent twice the widths. The sub-panels “b” and “c” show finite volume spectrum at $M_\pi = 266$ MeV obtained with different choices of the lattice interpolating fields. We note that black symbols are identified as scattering states shown by horizontal lines, and there is not extra energy level corresponding to $Z_c^+(3900)$.

D0 Collaboration recently reported a narrow peak ($\Gamma \sim 22$ MeV) in the $B_s\pi^+$ invariant mass of their $p\bar{p}$ collision data⁵⁷, while the later LHCb measurements did not confirm the peak structure⁵⁸. This state, if exists, has an interesting exotic content with four different quark flavors $\bar{b}s\bar{d}u$. It strongly decays into a two-particle state $B_s\pi^+$ and lies significantly below other thresholds. Therefore the Lüscher formula can be applied rather straightforwardly. Lang *et al.* calculated the finite volume spectrum in Eq. (2) by numerical simulation near $M_{\pi, \text{phys}}$. The left panel of Fig. 3 compares it with an analytic estimate at $M_{\pi, \text{phys}}$ assuming the existence of $X(5568)$. The energy level corresponding to $X(5568)$ is missing in the simulation data. This disfavors the existence of $X(5568)$ in agreement with the LHCb measurement.

There has also been recent interesting progress for $Z_c^+(3900)$, another candidate for four quark exotic states. BESIII reported a peak structure slightly above the $\bar{D}D^*$ threshold in the $J/\psi\pi^+$ invariant mass distribution⁶⁰, which was also confirmed in Belle and CLEO-c data^{61,62}. The finite volume spectrum has already been studied^{55,63,64}. As shown in the right panel of Fig. 3, any extra energy level corresponding to Z_c has not been confirmed suggesting the possibility of the Z_c peak of kinematical origin. Recently, the scattering matrix among three states, J/ψ , $\bar{D}D^*$ and $\rho\eta_c$, has been determined at unphysical $M_\pi \gtrsim 410$ MeV by the HALQCD

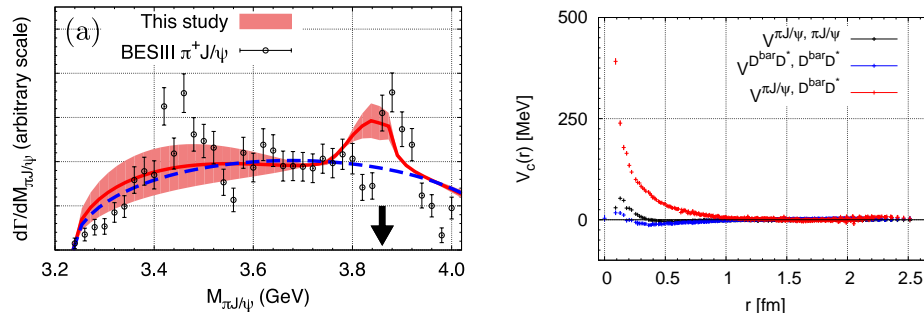


Fig. 4. Right panel: $J/\Psi\pi^+$ invariant mass distribution (figure from Ref. 59). Open circles are BESIII data⁶⁰. The vertical arrow indicates the Z_c peak position. The red band shows a theoretical estimate obtained from the scattering matrix by the HALQCD method. The peak structure disappears in the blue dashed line, which is obtained by turning off the off-diagonal potential. Left panel: coupled-channel potential among $J/\psi\pi$ and $\bar{D}D^*$ states (courtesy of Yoichi Ikeda (HALQCD Collaboration)). The black and blue symbols show the diagonal potentials of the $J/\psi\pi$ and $\bar{D}D^*$ states, respectively. The off-diagonal potential between these states is plotted by the red symbol.

method⁵⁹. As shown in the left panel of Fig. 4, it reproduces the Z_c peak structure, which however disappears by turning off the strong coupling between $J/\psi\pi$ and $\bar{D}D^*$ shown in the right panel. This suggests that the Z_c peak is a threshold cusp effect due to the opening of the $\bar{D}D^*$ threshold. This interesting observation should be confirmed at $M_{\pi, \text{phys}}$, since unphysically heavy M_π significantly disorders possibly relevant thresholds $\psi_{\{2S, 1D, 3\}}\pi$. A coupled-channel analysis using the Lüscher formula is also welcome to firmly establish the origin of the Z_c peak structure.

3. Flavor physics

There has been steady progress in precision lattice study of the (semi)leptonic decays and neutral meson mixings. These processes provide determination of relevant Cabibbo-Kobayashi-Maskawa (CKM) matrix elements and a wealth of probes of new physics, such as the fully differential decay distribution. For processes where we can safely ignore the final state interaction, the relevant hadronic matrix elements and hadronic inputs can be straightforwardly calculated from correlation functions on the lattice. For the kaon leptonic decay, for instance, the amplitude Z_H of the two-point function (1) of the weak axial current $\mathcal{O}_H = A_4$ gives the matrix element $\langle 0|A_4|K(p)\rangle = M_K f_K$, which is parametrized by the kaon decay constant f_K . Form factors for semileptonic decays and bag parameters for neutral meson mixings can be similarly extracted from tree-point functions. This is rather straightforward procedure, and hence good simulation setup, namely the choice of the lattice formulation and simulation parameters, is a key to perform a high precision calculation.

There have been many independent studies on sufficiently large and fine lattices

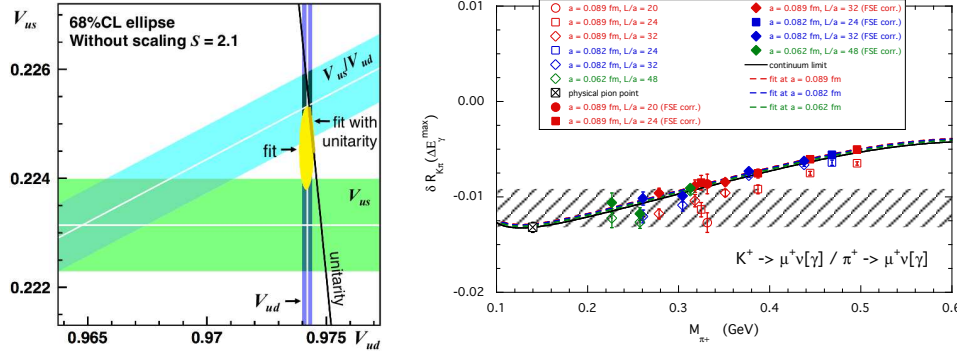


Fig. 5. Left panel: test of CKM unitarity in $(|V_{ud}|, |V_{us}|)$ plane (figure from Ref. 69). The horizontal and oblique bands indicate $|V_{us}|$ determined from the $K \rightarrow \pi \ell \nu$ decay and $|V_{us}/V_{ud}|$ from the kaon and pion leptonic decays, respectively. The vertical band is $|V_{ud}|$ from the super-allowed nuclear β decays. A fit to these data yields $(|V_{ud}|, |V_{us}|)$ shown in the yellow region. The black solid line satisfies CKM unitarity in the first row, where $|V_{ub}|$ has small effects. Right panel: isospin correction $\delta R_{K\pi}$ to $\Gamma(K \rightarrow \ell \nu)/\Gamma(\pi \rightarrow \ell \nu)$ (figure from Ref. 70). Symbols show lattice data, whereas the dashed and solid lines are their fit curves at finite lattice spacings and in the continuum limit, respectively. The shaded band represents the ChPT estimate^{71,72}.

near $M_{\pi, \text{phys}}$ for the kaon (semi)leptonic decay and mixing. For instance, the current accuracy reaches the sub% level for the $K \rightarrow \pi$ form factor and the ratio of the kaon and pion decay constants f_K/f_π ⁶⁵. These hadronic inputs are used to precisely determine $|V_{us}|$ and $|V_{us}/V_{ud}|$ as shown in the left panel of Fig. 5. Together with $|V_{ud}|$ from the super-allowed nuclear β decays, CKM unitarity in the first row $|V_{ud}|^2 + |V_{us}|^2 + |V_{ub}|^2 = 1$ is now confirmed at the 0.1% level⁶⁶. This is one of the most precise unitarity test, and can probe the new physics scale up to ≈ 10 TeV^{67,68}.

At the impressive accuracy of the hadronic inputs, the uncertainty of the EM and strong isospin breaking corrections to the decay rate is no longer negligible. These corrections have been conventionally estimated in chiral perturbation theory (ChPT) with typical accuracy of 0.2–0.4%⁷³. It is however difficult to improve the ChPT calculation by extending to higher orders, where many additional unknown low energy constants appear. Lattice QCD calculation of these corrections takes on increasing importance and is being actively pursued⁵. The presence of the infrared divergences complicates the calculation of the EM corrections for the (semi) leptonic decays. Recently, a new strategy was proposed⁷⁴ and successfully applied to the leptonic decay rate ratio $\Gamma(K \rightarrow \ell \nu)/\Gamma(\pi \rightarrow \ell \nu)$, which provides the determination of $|V_{us}|/|V_{ud}|$. As shown in the right panel of Fig. 5, their preliminary estimate $\delta R_{K\pi} = -0.0137(13)$ ⁷⁰ is in good agreement with the conventional ChPT estimate $-0.0112(21)$ ^{71,72}. The lattice estimate is, however, systematically improvable by more realistic simulations, for instance, near $M_{\pi, \text{phys}}$ with higher statistics.

Another thrust of recent lattice efforts in kaon physics is application to more involved processes, such as the $K \rightarrow \pi\pi$ hadronic decay and rare decays. Similar

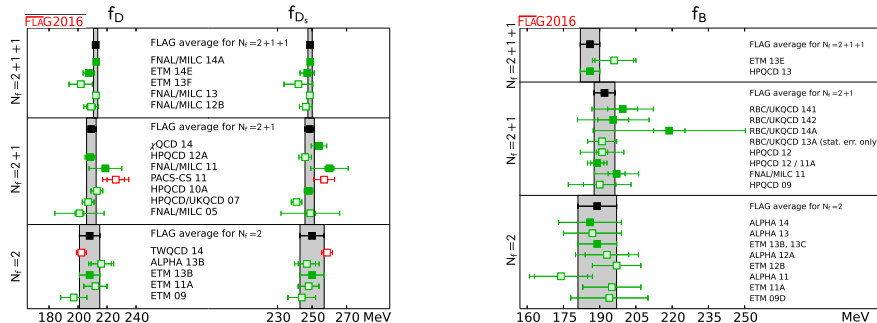


Fig. 6. Compilation of recent lattice results for heavy-light decay constants f_D , f_{D_s} (left panel) and f_B (right panel) (figures from the FLAG review⁶⁵). Green symbols are obtained with systematics under control, whereas reds are not. Black squares are average of the filled symbols at each N_f , that is the number of flavors of dynamical quarks.

to the scattering amplitudes discussed in Sec. 2, the $K \rightarrow \pi\pi$ decay amplitudes are not directly given by the correlation functions on the lattice. Lellouch and Lüscher derived a formula to relate the finite volume matrix elements to the physical amplitudes⁷⁵. This has been successfully implemented in recent works by the RBC/UKQCD Collaborations for the $\Delta I = 3/2$ ⁷⁶ and $1/2$ ⁷⁷ channels. They obtain the direct CP violation parameter $\text{re}[e'/\epsilon] = 1.4(5.2)_{\text{stat}}(4.6)_{\text{sys}} \times 10^{-4}$. A less precise but consistent value $8(25)_{\text{stat}} \times 10^{-4}$ was obtained by an independent calculation with a different lattice formulation⁷⁸. A slight tension with the experimental value^{79–81} $16.6(2.3) \times 10^{-4}$ is of great phenomenological interest^{82,83}. The RBC/UKQCD Collaboration is making continuous efforts, which aim improved statistical accuracy of a factor of two⁸⁴, and better control of leading systematic uncertainties, for instance, due to the operator renormalization⁸⁵. We can therefore hope an improved estimate of $\text{re}[e'/\epsilon]$ in the near future. Note also that a first exploratory study is available both for $K \rightarrow \pi\ell^+\ell^-$ ⁸⁶ and $K \rightarrow \pi\nu\bar{\nu}$ ⁸⁷ decays.

The accuracy of the heavy-light meson decay constants has been significantly improved over the past several years. Figure 6 shows that there have been many independent calculations with systematics under control. The accuracy of the world average quoted by the Flavor Lattice Averaging Group (FLAG)⁶⁵ is $\approx 0.6\%$ for $f_{D_{(s)}}$ and $\approx 2\%$ for $f_{B_{(s)}}$. These are well below the current experimental precision⁸⁸, and the isospin correction starts being relevant at this level of accuracy.

The $B \rightarrow \pi\ell\nu$ and $B \rightarrow D^{(*)}\ell\nu$ semileptonic decays provide the conventional determination of the CKM matrix elements $|V_{ub}|$ and $|V_{cb}|$, respectively. As shown in Fig. 7, however, there has been a long-standing tension between these exclusive and inclusive decays⁸⁸. While this could be a sign of new physics⁸⁹, we clearly need more thorough theoretical and experimental studies to fully resolve/understand the tension. Lattice QCD plays a crucial role in controlling the dominant theoretical uncertainty arising from the relevant hadronic matrix elements.

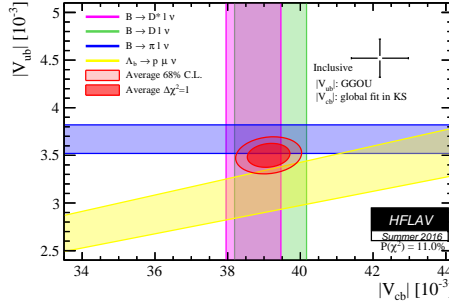


Fig. 7. $|V_{ub}|$ versus $|V_{cb}|$ (figure from Ref. 88). Horizontal and vertical bands represent $|V_{ub}|$ from $B \rightarrow \pi \ell \nu$ and $|V_{cb}|$ from $B \rightarrow D^{(*)} \ell \nu$, respectively. The oblique band is $|V_{ub}|/|V_{cb}|$ from $\Lambda_b \rightarrow p \ell \nu$ and $\Lambda_c \ell \nu$. The average of these estimates is shown by the red region. These should be compared with the point with the error bars obtained from the inclusive decays $B \rightarrow X_{u(c)} \ell \nu$.

In the SM, the $B \rightarrow \pi \ell \nu$ and $B \rightarrow D \ell \nu$ decays proceed only through the weak vector current V_μ due to parity symmetry. The matrix element for $B \rightarrow \pi \ell \nu$, for instance, is parametrized by two form factors as

$$\langle \pi(p') | V_\mu | B(p) \rangle = \left\{ p + p' - \frac{M_B^2 - M_\pi^2}{q^2} \pi \right\}_\mu f_+^{B\pi}(q^2) + \frac{M_B^2 - M_\pi^2}{q^2} q_\mu f_0^{B\pi}(q^2), \quad (3)$$

where $q^2 = (p - p')^2$ is the momentum transfer to the lepton pair $\ell \nu$. For $\ell = e, \mu$, the contribution from the “ f_0 term” to the differential decays rate $d\Gamma/dq^2$ is suppressed by m_ℓ^2 . Hence the experimental value of $|V_{ub}| f_+^{B\pi}(q^2)$ can be obtained from $d\Gamma/dq^2$. A simultaneous fit to the experimental data and $f_+^{B\pi}$ from lattice QCD determines

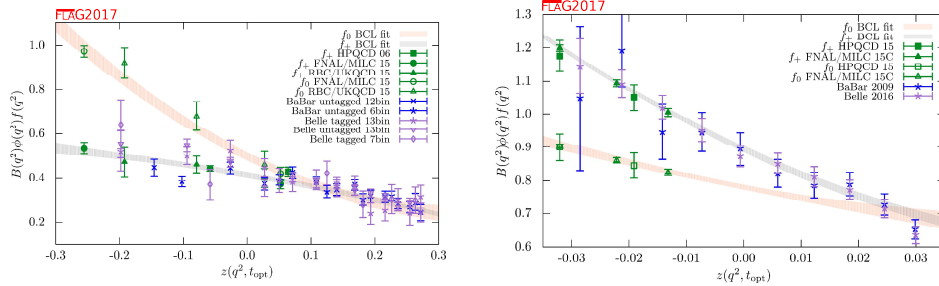


Fig. 8. Simultaneous fits to determine $|V_{ub}|$ from $B \rightarrow \pi \ell \nu$ (left panel) and $|V_{cb}|$ from $B \rightarrow D \ell \nu$ (right panel) (figures from Ref. 65). Recent lattice results for $f_+^{B\pi(BD)}(q^2)$ ^{90–94} and $|V_{ub(cb)}| f_+^{B\pi(BD)}(q^2)$ from BaBar^{95–97} and Belle^{98–100} are fitted into a model-independent parametrization in terms of z -parameter defined as $z(q^2, t_{\text{opt}}) = (\sqrt{t_+ - q^2} - \sqrt{t_+ - t_{\text{opt}}}) / (\sqrt{t_+ - q^2} + \sqrt{t_+ - t_{\text{opt}}})$. Here t_+ is the threshold $t_+ = (M_B + M_{\pi(D)})^2$ and a tunable parameter t_{opt} is set to $(M_B + M_{\pi(D)})(\sqrt{M_B} - \sqrt{M_{\pi(D)}})^2$ to minimize the maximal value of $|z|$. We note that lattice data of f_0 are also included into the fits to make use of the kinematical constraint $f_+(0) = f_0(0)$.

$|V_{ub}|$ as a relative normalization factor. The same manner is used to determine $|V_{cb}|$ from $B \rightarrow D\ell\nu$ and can apply to alternative determinations discussed below. We also note that it has been customary to use a model-independent parametrization based on the analyticity of the form factors to describe their q^2 dependence¹⁰¹. Figure 8 shows FLAG's analysis using recent lattice results for $B \rightarrow \pi$ ⁹⁰⁻⁹² and $B \rightarrow D$ ^{93,94}. While the state-of-the-art calculations start to achieve good accuracy competitive to experiments, the number of such calculations are still rather limited and independent calculations are highly welcome^{102,103}.

The analysis of $B \rightarrow D^*\ell\nu$ is more involved, since it proceeds also through the weak axial current, and have four form factors. The previous lattice study¹⁰⁴ focused the zero recoil limit, where $d\Gamma/dq^2$ is described by a single form factor in

$$\langle D^*(\epsilon, p') | A_\mu | B(p) \rangle = 2i\sqrt{M_B M_{D^*}} \epsilon_\mu h_{A_1} \quad (\mathbf{p} = \mathbf{p}' = \mathbf{0}). \quad (4)$$

Here ϵ is the polarization vector of D^* . The conventional determination of $|V_{cb}|$ relies on a parametrization based on heavy quark symmetry to constrain the form factors at non-zero recoils¹⁰⁵. It is, however, recently argued the possibility that uncertainty due to the parametrization is not fully understood¹⁰⁶⁻¹⁰⁸. In order to resolve the tension in $|V_{cb}|$, lattice calculation of all form factors at non-zero recoil is crucial, and the first preliminary analysis was recently reported by the Fermilab/MILC Collaboration¹⁰⁹.

Lattice QCD is actively exploring alternative decay modes, which may elucidate the tension in $|V_{\{ub,cb\}}|$. Modern calculations are available for $B_s \rightarrow K\ell\nu$ by the HPQCD¹¹¹, RBC/UKQCD⁹¹ and ALPHA¹¹² Collaborations, and for $B_s \rightarrow D_s\ell\nu$ by the Fermilab/MILC¹¹³, ETM¹¹⁴ and HPQCD¹¹⁰ Collaborations. Simulation techniques for $B \rightarrow \{\pi, D^{(*)}\}\ell\nu$ can be straightforwardly applied to attain a similar level of precision as seen in the right panel of Fig. 9. The left panel shows that

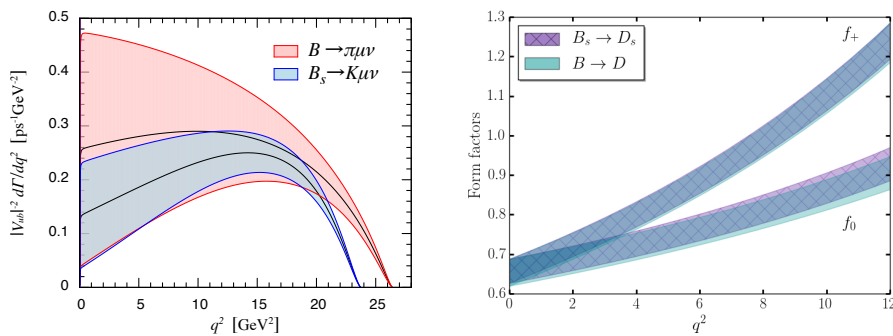


Fig. 9. Left panel: differential decay rates for $B_s \rightarrow K\mu\nu$ (blue band) and $B \rightarrow \pi\mu\nu$ (red band) predicted by using recent lattice estimate of relevant form factors (figure from Ref. 91). Right panel: vector (f_+) and scalar (f_0) form factors for $B_s \rightarrow D_s\ell\nu$ (shaded dark blue band) and $B \rightarrow D\ell\nu$ (shaded pale blue band) decays (figure from Ref. 110).

the theoretical accuracy is better for $B_s \rightarrow K\ell\nu$ than $B \rightarrow \pi\ell\nu$, since having the (heavier) kaon instead of the pion reduces the statistical fluctuation and light quark mass dependence of the form factors. The latter is advantageous to control the chiral extrapolation. Therefore, the most crucial issue for the practical use of these alternative modes is the experimental feasibility of precise measurements of $d\Gamma/dq^2$.

Baryon decays also provide the alternative determination of the CKM matrix elements. The first lattice calculation of $\Lambda_b \rightarrow p\ell\nu$ and $\Lambda_b \rightarrow \Lambda_c\ell\nu$ form factors at the physical b quark mass obtained $|V_{ub}|/|V_{cb}|$ shown in Fig. 7¹¹⁵. An example of the relevant form factors is shown in the left panels of Fig. 10. Recently, the first study of $\Lambda_c \rightarrow \Lambda\ell\nu$ yields $|V_{cs}|$ consistent with those from D meson decays¹¹⁶. However baryons are known to be more challenging in controlling systematics, in particular finite volume effects and chiral extrapolation. Since the target accuracy for $|V_{\{cb,cs\}}|$ is high, more thorough study of systematics is recommended to firmly establish the CKM matrix elements from the baryon decays.

For rare decays, however, such theoretical uncertainty could be well below the experimental one. Reference 117 recently presented the first calculation of all ten form factors for $\Lambda_b \rightarrow \Lambda\ell\ell$. This decay may shed new light on the so-called $B \rightarrow K^*\ell\ell$ anomaly, namely more than 3σ tension in its angular distribution¹¹⁹, since these two decays share the $b \rightarrow s\ell\ell$ effective weak Hamiltonian. As shown in the right panel of Fig. 10, the SM prediction and the LHCb result¹¹⁸ show reasonable consistency for the differential branching fraction. A simple scenario for the $B \rightarrow K^*\ell\ell$ anomaly, namely a negative new physics coupling for an effective interaction $(\bar{s}_L\gamma_\mu b_L)(\bar{\ell}\gamma^\mu\ell)$, worsens this consistency. Therefore the authors suggest that the $B \rightarrow K^*\ell\ell$ anomaly

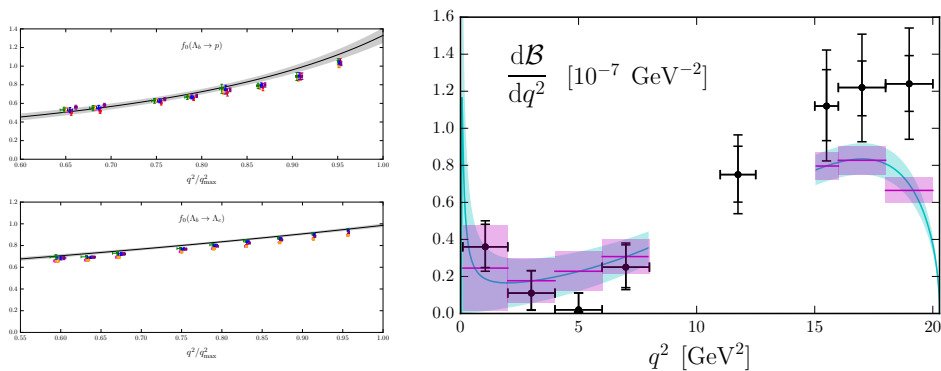


Fig. 10. Left panels: an example of $\Lambda_b \rightarrow p$ (left top panel) and $\Lambda_b \rightarrow \Lambda_c$ (left bottom panel) form factors describing matrix elements $\langle p(\Lambda_c)|V_\mu|\Lambda_b\rangle$ (figure from Ref. 115). The horizontal axis represents q^2 normalized by $q_{\text{max}}^2 = (M_{\Lambda_b} - M_{p(\Lambda_c)})^2$. Right panel: differential branching fraction of $\Lambda_b \rightarrow \Lambda\ell\ell$ as a function of q^2 (figure from Ref. 117). The black circle shows the LHCb result¹¹⁸ with two error bars including and excluding the uncertainty from the normalization mode $\Lambda_b \rightarrow J/\Psi\Lambda$. The continuous blue band is the SM prediction as a function of q^2 , whereas magenta band show the average at each q^2 bin.

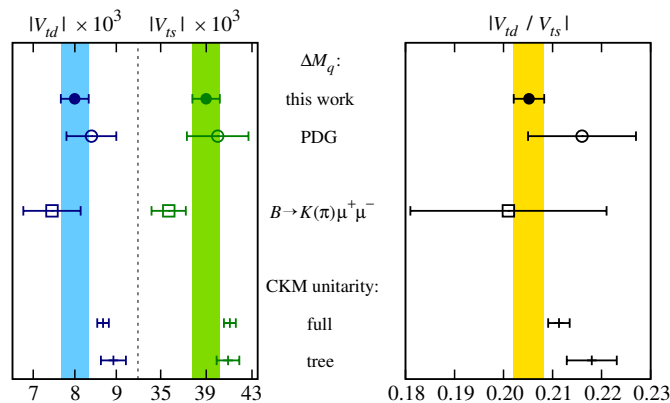


Fig. 11. Comparison of $|V_{td}|$ and $|V_{ts}|$ (left panel) and their ratio (right panel) (figure from Ref. 120). The filled circles and vertical bands show the Fermilab/MILC's estimate through the neutral $B_{(s)}$ meson mass difference ΔM_q , which shows a 2–3 times reduction of the uncertainty upon the previous estimate (open circles). The squares are from the rare decays $B \rightarrow K(\pi)\mu\mu$. The plus symbols are obtained by assuming CKM unitarity through a global fit to all available inputs and a fit limited to inputs from tree-level processes.

is due to incomplete treatment of the charmonium resonance contribution ($B \rightarrow K^*\psi_n(\rightarrow ll)$, $\psi_1 = J/\psi$, $\psi_2 = \psi_{2S}$, ...) in the angular analysis.

For the neutral B meson mixing, the Fermilab/MILC Collaboration recently published a precise calculation of all matrix elements in and beyond the SM¹²⁰. High statistics, realistic simulation parameters (a and M_π), and a better implementation of the renormalization of four-fermion lattice operators^{120,121} led to 2–3 times improvement in the relevant CKM elements as shown in Fig. 11. With such high precision, a tantalizing tension with CKM unitarity emerges. We also note that there is a tension in a matrix element beyond the SM with ETM Collaborations' result in $N_f = 2$ QCD¹²². We hope that independent precision calculations will clarify the source of these tensions in the near future.

While generalization of the Lellouch-Luscher framework is actively pursued, it is not yet sufficient to allow lattice simulations of hadronic B or D decays which have various multi-particle final states. However, lattice simulation is now being applied to inclusive decays^{124–127}, which are summed over all possible hadronic final states. For the hadronic τ decays $\tau \rightarrow X_s\nu$, for instance, the optical and Cauchy theorems relate a normalized decay rate R_s to a contour integral of the weak current correlator over the complex energy variable s

$$R_s = \frac{\Gamma(\tau \rightarrow X_s\nu_\tau)}{\Gamma(\tau \rightarrow e\bar{\nu}_e\nu_\tau)} = -\frac{1}{2\pi i} |V_{us}|^2 \oint_{|s|=s_0} ds w(s) \langle 0 | J_\mu J_\mu | 0 \rangle. \quad (5)$$

Here, s_0 and $w(s)$ are appropriately chosen parameter and weight function, and J_μ represents the relevant weak current. By employing a pole type weight function

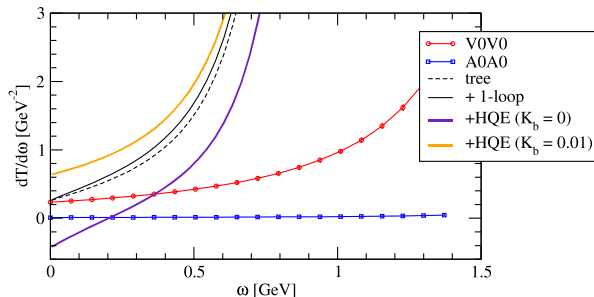


Fig. 12. First derivative of the matrix element $T_{\mu\nu}$ as a function of kinematical variable $\omega = M_B - q_0$. Red circles and Blue squares are weak vector ($J_\mu = V_\mu$) and axial vector ($J_\mu = A_\mu$) current contributions, respectively. Here we plot $dT_{\mu\nu}/d\omega$ instead of $T_{\mu\nu}$ itself to avoid contamination from contact terms. Thin black dashed line shows the estimate from the heavy quark expansion at the leading order in α_s and $1/m_b$, whereas the one-loop correction is included into the black solid line. The thick lines take account of the $1/m_b$ correction with two choices of the non-perturbative input $K_b = -\langle B|\bar{b}(iD)^2b|B\rangle/(2m_b^2)$ ¹²³.

$w(s) = 1/\Pi_{n=1}^N(s + Q_n^2)$ ($Q_n^2 > 0$), the integral can be evaluated by the current correlator at space like points $s = -Q_1^2, \dots, -Q_N^2$, which can be precisely determined on the lattice. This is RBC/UKQCD's implementation to determine $|V_{us}|$ from the hadronic τ decays¹²⁴. They obtain $|V_{us}| = 0.223 - 0.225$ ^{128,129}, which is in good agreement with those from the kaon decays shown in the left panel of Fig. 5.

Inclusive semileptonic B decays are more involved but important application to resolve the discrepancy in $|V_{\{ub,cb\}}|$ from the exclusive decays¹²⁵. Through the optical theorem, the hadronic part of the inclusive decay amplitude can be related to a forward scattering matrix element

$$T_{\mu\nu} = i \int d^4x e^{-iqx} \frac{1}{2M_B} \langle B|T [J_\mu^\dagger(x)J_\nu(0)]|B\rangle. \quad (6)$$

A preliminary analysis for $B \rightarrow X_c \ell \nu$ at zero recoil has been reported by Hashimoto *et al.* in Ref. 130. Figure 12 compares the matrix element $T_{\mu\nu}$ between lattice QCD and the heavy quark expansion (HQE) used in the conventional inclusive determination of $|V_{cb}|$. They are reasonably consistent in the perturbative region of a kinematical variable $\omega = M_B - q_0 \sim 0$. However, they deviate from each other towards large ω , where the perturbation series is reasonably convergent, but the $1/m_b$ correction has substantial uncertainty due to the choice of the non-perturbative input. Further quantitative test of the HQE and detailed comparison between the inclusive and exclusive determinations on the same lattice may give us a hint to resolve the tension in $|V_{\{ub,cb\}}|$.

4. Muon anomalous magnetic moment

The past several years have witnessed rapid progress in calculating the muon anomalous magnetic moment $a_\mu = (g-2)/2$ on the lattice. This quantity is known to great

precision ≈ 0.5 ppm both in the SM^{131–133} and experiment¹³⁴. Their 3–4 σ deviation may be a signal of new physics. New experiments, E989 at Fermilab¹³⁵ and E34 at J-PARC¹³⁶, aim to improve the experimental accuracy by a factor of four. On the theory side, the accuracy is currently limited by hadronic uncertainties coming from the hadronic vacuum polarization (HVP) and hadronic light-by-light (HLbL) contributions shown in Fig. 13. The former has been most precisely calculated from the dispersive analysis^{131–133} of experimental data of the so-called R -ratio $\sigma(e^+e^- \rightarrow \text{hadrons})/\sigma_{\text{tree}}(e^+e^- \rightarrow \mu^+\mu^-)$. A similar dispersive approach is under development^{137–139}, and model estimates are currently quoted for the HLbL^{140–142}. An ultimate goal of recent lattice efforts is to provide the first-principle prediction for these hadronic contributions with reduced uncertainty.

The leading order HVP contribution a_μ^{HVP} is expressed as an integral over the Euclidean momentum Q^2 ^{143,144}

$$a_\mu^{\text{HVP}} = 4\alpha^2 \int_0^\infty dQ^2 K(Q^2, m_\mu^2) \hat{\Pi}(Q^2), \quad \hat{\Pi}(Q^2) = \Pi(Q^2) - \Pi(0), \quad (7)$$

where K is a known weight. In pioneering works^{144–147}, the vacuum polarization function $\Pi(Q^2)$ was straightforwardly calculated from the EM current correlator

$$(Q_\mu Q_\nu - \delta_{\mu\nu} Q^2) \Pi(Q^2) = \int d^4x e^{iQx} \langle J_\mu^{\text{EM}}(x) J_\nu^{\text{EM}}(0) \rangle. \quad (8)$$

It was later suggested^{148–150} that $\hat{\Pi}(Q^2)$ can be expressed using the correlator $G(t) = \sum_{\mathbf{x}} \langle J_\mu^{\text{EM}}(\mathbf{x}, t) J_\mu^{\text{EM}}(0) \rangle$ with zero spatial momentum, which is less noisy than the right-handed side of (8). a_μ^{HVP} is written as an integral over the Euclidean time

$$a_\mu^{\text{HVP}} = 4\alpha^2 \int_0^\infty dt \tilde{K}(t, m_\mu^2) G(t), \quad (9)$$

which is often employed in recent lattice studies^{151–153}. We note that the integral (7) receives large contribution from the infrared regime $Q^2 \approx O(m_\mu^2)$. References

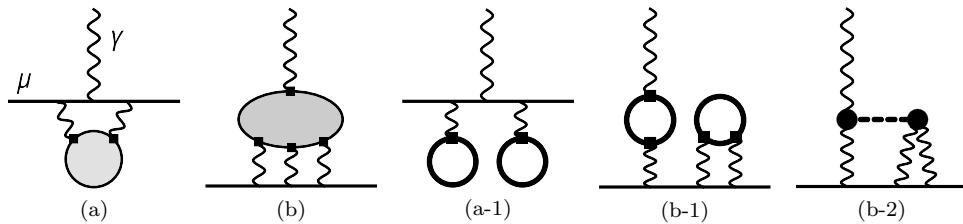


Fig. 13. The leading HVP (a) and HLbL (b) contributions to a_μ . Wavy and solid lines represent the photon and muon propagators, respectively. The shaded circle for the HVP (HLbL) is the two- (four-)point function of the quark EM current J_μ^{EM} (squares) in QCD. (a-1) An example of quark-disconnected diagrams for the HVP. Two quark loops (thick lines) are connected by gluons. (b-1) An example of leading disconnected diagrams for the HLbL. We note that a quark loop with a single J_μ^{EM} vertex vanishes in the SU(3) limit, since the up, down and strange quark charges sum up to zero. (b-2) The π^0 contribution to the HLbL. The thick dashed line and the solid circles represent the π^0 propagator and $\pi^0 \rightarrow \gamma^* \gamma^*$ transition form factor, respectively.

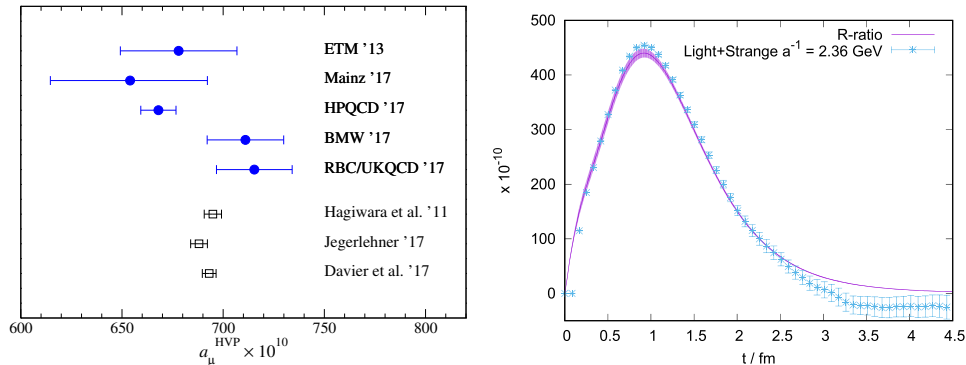


Fig. 14. Left panel: recent lattice estimates of a_μ^{HVP} (blue solid circles)^{151–153,157,158}. We also plot a_μ^{HVP} from the dispersive method^{131–133}. Right panel: comparison of integrand $\hat{K}(t, m_\mu^2)G(t)$ in Eq.(9) (figure from Ref. 12). The crosses are lattice data at a finite lattice spacing $a \sim 0.08$ fm, whereas the band is obtained from the experimental data of the R -ratio.

154–156 employ another strategy, which reconstructs $\hat{\Pi}(Q^2)$ in the infrared region by using its derivatives at $Q^2=0$ calculated from time moments $G_{2n} = \sum_t t^{2n} G(t) = (-1)^n \left(\partial^{2n} Q^2 \hat{\Pi}(Q^2) / \partial Q^{2n} \right)_{Q^2=0}$.

The challenge in the lattice calculation of a_μ^{HVP} is to control all uncertainties below 1% to compete with the current best estimate from the R -ratio. The dominant contribution comes from the connected diagram with the light quark current $(2/3)\bar{u}\gamma_\mu u - (1/2)\bar{d}\gamma_\mu d$. It has been calculated in the isospin limit with controlled continuum and chiral extrapolations^{147,151–153,156,157}, whereas finite volume effects are corrected by employing effective field theories or directly examined by simulating multiple volumes. Possible corrections have been studied: strong isospin breaking^{153,158}, EM correction^{153,159}, disconnected diagrams (Fig. 13 (a-1))^{151,152,155,160}, strange and charm quark contributions^{151,152,154,159,161}. It is confirmed that bottom quarks have small effects¹⁶². Thanks to these substantial efforts, the current lattice accuracy for a_μ^{HVP} has reached a few % level as summarized in Fig. 14^a.

Currently, a largest uncertainty is the statistical fluctuation, though $G(t)$ is less noisy compared to the multi-particle correlators discussed in Sec. 2 and three- and four-point functions in Sec. 3. A better control in the infrared region, namely small Q^2 and large t , is a crucial issue towards a more precise determination and is being actively studied^{151,156,163–166}. Another interesting possibility is to combine $G(t)$ on the lattice and experimental R -ratio data. The time integral (9) is decomposed into $a_\mu^{\text{HVP}} = a_{\mu,\text{SD}}^{\text{HVP}} + a_{\mu,\text{ID}}^{\text{HVP}} + a_{\mu,\text{LD}}^{\text{HVP}}$. The R -ratio is then used to evaluate the short ($a_{\mu,\text{SD}}^{\text{HVP}}$) and long ($a_{\mu,\text{LD}}^{\text{HVP}}$) distance contributions to avoid possibly large discretization effects

^a Here we quote results from Refs. 152,153,158 published after this symposium. Their preliminary results had been available beforehand at the *35th International Symposium on Lattice Field Theory (Lattice 2017)*.

and statistical fluctuation, respectively. In the intermediate region, $a_{\mu, \text{ID}}^{\text{HVP}}$ can be calculated from $G(t)$. This combined analysis in Ref. 153 demonstrates good consistency in the integrand of Eq. (9) between lattice and experimental data (Fig. 14), and led to a most precise estimate $a_{\mu}^{\text{HVP}} = 692.5(2.7) \times 10^{-10}$. Simulating finer lattices and better control of the statistical accuracy can expand the intermediate t window, and will eventually lead to a pure theoretical estimate of a_{μ}^{HVP} with reduced uncertainty.

There has also been remarkable progress in the lattice calculation of a_{μ}^{HLbL} . Theoretical calculation thereof is challenging, because the relevant four-point function of J_{μ}^{EM} involves many connected and disconnected diagrams. There have recently been two approaches to calculate presumably dominant contributions. Reference 167 focuses on the connected and leading disconnected diagrams which survive in the SU(3) limit (Fig. 13 (b-1)). With algorithmic improvements¹⁶⁸, they obtain statistically significant estimate $a_{\mu}^{\text{HLbL}} = 5.4(1.4) \times 10^{-10}$ at the physical point $M_{\pi, \text{phys}}$ but at a single lattice spacing. Another approach in Ref. 169 estimates presumably dominant π^0 contribution (Fig. 13 (b-2)) through the lattice calculation of the $\pi^0 \rightarrow \gamma^* \gamma^*$ form factor, and yields $a_{\mu}^{\text{HLbL}} = 6.5(0.8) \times 10^{-10}$. While the quote errors are statistical only, the reasonable agreement between the different approaches is encouraging and motivates more realistic simulations and surveys of systematics, particularly finite volume effects due to massless photons on the lattice¹⁷⁰.

5. Conclusions

In this review, we have presented highlights of recent progress on hadron spectrum and flavor physics from lattice QCD. Masses and transition amplitudes can be straightforwardly calculated from lattice correlation functions for hadrons stable under QCD. Recent realistic simulations can yield deep insight into the nature of yet-unestablished states as in the case of Ξ_{cc} . Decay constants, kaon semileptonic form factors and bag parameters are now calculated with fully controlled uncertainties, and lie at the precision frontier of lattice QCD, where isospin corrections are being studied. The number of the precision calculations is currently rather limited for heavy hadron form factors and bag parameters. However, we can expect more independent calculations in the next few years.

Lattice QCD is now ready to study coupled-channel two-body scatterings. This leads to recent interesting progress on light resonances, σ , κ , ρ and K^* as well as heavy exotics such as $X(5568)$ and $Z_c(3900)$. These studies are however often limited to unphysically heavy pion masses, which significantly raise thresholds including pions and may turn resonances into bound-states. While such studies deepen our understanding of the existence form of the hadrons, simulating the physical pion mass is recommended in order to make a direct comparison with experiment.

There has been continuous progress on $K \rightarrow \pi\pi$ leading to slight tension with experiment, which is of great phenomenological interest. General framework to deal with three-particle states is necessary for hadronic B and D decays and un-

der active development. However, it was proposed that inclusive decays can be straightforwardly studied without such framework. This may offer useful hints to resolve long-standing tension in $|V_{ub}|$ and $|V_{cb}|$ between the exclusive and inclusive determinations.

Acknowledgments

I would like to thank Sinya Aoki, Shoji Hashimoto and Yoichi Ikeda for informative communications and assistance in preparing my talk and this manuscript.

References

1. S. Dürr *et al.* (BMW Collaboration), *Science* 322 (2008) 1224–1227, arXiv:0906.3599 [hep-lat].
2. S. Aoki *et al.* (PACS-CS Collaboration), *Phys. Rev. D* 79 (2009) 034503, arXiv:0807.1661 [hep-lat].
3. A. Bazavov *et al.* (MILC Collaboration), *Rev. Mod. Phys.* 82 (2010) 1349–1417, arXiv:0903.3598 [hep-lat].
4. W. Bietenholz *et al.* (QCDSF/UKQCD Collaboration), *Phys. Rev. D* 84 (2011) 054509, arXiv:1102.5300 [hep-lat].
5. A. Patella, PoS LATTICE2016 (2017) 020, arXiv:1702.03857 [hep-lat].
6. S. Borsanyi *et al.*, *Science* 347 (2015) 1452–1455, arXiv:1406.4088 [hep-lat].
7. R. Horsley *et al.*, *J. Phys. G* 43 (2016) 10LT02, arXiv:1508.06401 [hep-lat].
8. L. Maiani and M. Testa, *Phys. Lett. B* 245 (1990) 585–590.
9. C. Liu, PoS LATTICE2016 (2017) 006, arXiv:1612.00103 [hep-lat].
10. D. J. Wilson, PoS LATTICE2016 (2016) 016, arXiv:1611.07281 [hep-lat].
11. X. Feng, EPJ Web Conf. 175 (2018) 01005, arXiv:1711.05648 [hep-lat].
12. C. Lehner, EPJ Web Conf. 175 (2018) 01024, arXiv:1710.06874 [hep-lat].
13. G. Colangelo, M. Hoferichter, M. Procura, and P. Stoffer, EPJ Web Conf. 175 (2018) 01025, arXiv:1711.00281 [hep-ph].
14. P. Prez-Rubio, S. Collins, and G. S. Bali, *Phys. Rev. D* 92 (2015) 034504, arXiv:1503.08440 [hep-lat].
15. H. Na and S. A. Gottlieb, PoS LATTICE2007 (2007) 124, arXiv:0710.1422 [hep-lat].
16. L. Liu, H.-W. Lin, K. Orginos, and A. Walker-Loud, *Phys. Rev. D* 81 (2010) 094505, arXiv:0909.3294 [hep-lat].
17. S. Basak, S. Datta, M. Padmanath, P. Majumdar, and N. Mathur, PoS LATTICE2012 (2012) 141, arXiv:1211.6277 [hep-lat].
18. S. Dürr, G. Koutsou, and T. Lippert, *Phys. Rev. D* 86 (2012) 114514, arXiv:1208.6270 [hep-lat].
19. Y. Namekawa *et al.* (PACS-CS Collaboration), *Phys. Rev. D* 87 (2013) 094512, arXiv:1301.4743 [hep-lat].
20. Z. S. Brown, W. Detmold, S. Meinel, and K. Orginos, *Phys. Rev. D* 90 (2014) 094507, arXiv:1409.0497 [hep-lat].
21. M. Padmanath, R. G. Edwards, N. Mathur, and M. Peardon, *Phys. Rev. D* 91 (2015) 094502, arXiv:1502.01845 [hep-lat].
22. R. Aaij *et al.* (LHCb Collaboration), *Phys. Rev. Lett.* 119 (2017) 112001, arXiv:1707.01621 [hep-ex].
23. V. V. Kiselev, A. K. Likhoded, and A. I. Onishchenko, *Phys. Rev. D* 60 (1999) 014007, arXiv:hep-ph/9807354.

24. M. Mattson *et al.* (SELEX Collaboration), Phys. Rev. Lett. 89 (2002) 112001, arXiv:hep-ex/0208014.
25. A. Ocherashvili *et al.* (SELEX Collaboration), Phys. Lett. B628 (2005) 18–24, arXiv:hep-ex/0406033.
26. J. S. Russ (SELEX Collaboration), arXiv:hep-ex/0209075.
27. C.-W. Hwang and C.-H. Chung, Phys. Rev. D78 (2008) 073013, arXiv:0804.4044 [hep-ph].
28. B. Guberina, B. Melic, and H. Stefancic, Eur. Phys. J. C9 (1999) 213–219, arXiv:hep-ph/9901323.
29. M. Lüscher, Commun. Math. Phys. 105 (1986) 153–188.
30. M. Lüscher, Nucl. Phys. B354 (1991) 531–578.
31. M. Lüscher, Nucl. Phys. B364 (1991) 237–251.
32. N. Ishii, S. Aoki, and T. Hatsuda, Phys. Rev. Lett. 99 (2007) 022001, arXiv:nucl-th/0611096.
33. N. Ishii *et al.* (HALQCD Collaboration), Phys. Lett. B712 (2012) 437–441, arXiv:1203.3642 [hep-lat].
34. S. Aoki, B. Charron, T. Doi, T. Hatsuda, T. Inoue, and N. Ishii, Phys. Rev. D87 (2013) 034512, arXiv:1212.4896 [hep-lat].
35. G. S. Bali *et al.* (RQCD Collaboration), Phys. Rev. D93 (2016) 054509, arXiv:1512.08678 [hep-lat].
36. R. A. Briceño, J. J. Dudek, R. G. Edwards, and D. J. Wilson, Phys. Rev. Lett. 118 (2017) 022002, arXiv:1607.05900 [hep-ph].
37. K. Rummukainen and S. A. Gottlieb, Nucl. Phys. B450 (1995) 397–436, arXiv:hep-lat/9503028.
38. C. h. Kim, C. T. Sachrajda, and S. R. Sharpe, Nucl. Phys. B727 (2005) 218–243, arXiv:hep-lat/0507006.
39. N. H. Christ, C. Kim, and T. Yamazaki, Phys. Rev. D72 (2005) 114506, arXiv:hep-lat/0507009.
40. M. Lage, U.-G. Meissner, and A. Rusetsky, Phys. Lett. B681 (2009) 439–443, arXiv:0905.0069 [hep-lat].
41. S. He, X. Feng, and C. Liu, JHEP 07 (2005) 011, arXiv:hep-lat/0504019.
42. R. A. Briceño, Phys. Rev. D89 (2014) 074507, arXiv:1401.3312 [hep-lat].
43. C. E. Thomas (Hadron Spectrum Collaboration), EPJ Web Conf. 137 (2017) 01021.
44. D. Guo, A. Alexandru, R. Molina, and M. Döring, Phys. Rev. D94 (2016) 034501, arXiv:1605.03993 [hep-lat].
45. B. Hu, R. Molina, M. Döring, and A. Alexandru, Phys. Rev. Lett. 117 (2016) 122001, arXiv:1605.04823 [hep-lat].
46. D. J. Wilson, R. A. Briceño, J. J. Dudek, R. G. Edwards, and C. E. Thomas, Phys. Rev. D92 (2015) 094502, arXiv:1507.02599 [hep-ph].
47. Z. Fu and L. Wang, Phys. Rev. D94 (2016) 034505, arXiv:1608.07478 [hep-lat].
48. C. Alexandrou *et al.*, Phys. Rev. D96 (2017) 034525, arXiv:1704.05439 [hep-lat].
49. J. R. Peláez, Phys. Rept. 658 (2016) 1, arXiv:1510.00653 [hep-ph].
50. K. Polejaeva and A. Rusetsky, Eur. Phys. J. A48 (2012) 67, arXiv:1203.1241 [hep-lat].
51. M. T. Hansen and S. R. Sharpe, Phys. Rev. D86 (2012) 016007, arXiv:1204.0826 [hep-lat].
52. R. A. Briceño and Z. Davoudi, Phys. Rev. D88 (2013) 094507, arXiv:1204.1110 [hep-lat].
53. R. A. Briceño, M. T. Hansen, and S. R. Sharpe, Phys. Rev. D95 (2017) 074510, arXiv:1701.07465 [hep-lat].

54. C. B. Lang, D. Mohler, and S. Prelovsek, Phys. Rev. D94 (2016) 074509, arXiv:1607.03185 [hep-lat].
55. S. Prelovsek, C. B. Lang, L. Leskovec, and D. Mohler, Phys. Rev. D91 (2015) 014504, arXiv:1405.7623 [hep-lat].
56. N. Brambilla *et al.*, Eur. Phys. J. C74 (2014) 2981, arXiv:1404.3723 [hep-ph].
57. V. M. Abazov *et al.* (D0 Collaboration), Phys. Rev. Lett. 117 (2016) 022003, arXiv:1602.07588 [hep-ex].
58. R. Aaij *et al.* (LHCb Collaboration), Phys. Rev. Lett. 117 (2016) 152003, arXiv:1608.00435 [hep-ex].
59. Y. Ikeda *et al.* (HALQCD Collaboration), Phys. Rev. Lett. 117 (2016) 242001, arXiv:1602.03465 [hep-lat].
60. M. Ablikim *et al.* (BESIII Collaboration), Phys. Rev. Lett. 110 (2013) 252001, arXiv:1303.5949 [hep-ex].
61. Z. Q. Liu *et al.* (Belle Collaboration), Phys. Rev. Lett. 110 (2013) 252002, arXiv:1304.0121 [hep-ex].
62. T. Xiao, S. Dobbs, A. Tomaradze, and K. K. Seth, Phys. Lett. B727 (2013) 366–370, arXiv:1304.3036 [hep-ex].
63. Y. Chen *et al.*, Phys. Rev. D89 (2014) 094506, arXiv:1403.1318 [hep-lat].
64. S.-h. Lee, C. DeTar, H. Na, and D. Mohler (Fermilab/MILC Collaboration), arXiv:1411.1389 [hep-lat].
65. S. Aoki *et al.* (Flavour Lattice Averaging Group), Eur. Phys. J. C77 (2017) 112, arXiv:1607.00299 [hep-lat].
66. T. Kaneko, X.-R. Lyu, and A. Oyanguren, PoS CKM2016 (2017) 014, arXiv:1705.05975 [hep-ph].
67. V. Cirigliano, J. Jenkins, and M. Gonzalez-Alonso, Nucl. Phys. B830 (2010) 95–115, arXiv:0908.1754 [hep-ph].
68. M. Gonzalez-Alonso and J. Martin Camalich, JHEP 12 (2016) 052, arXiv:1605.07114 [hep-ph].
69. M. Moulson, PoS CKM2016 (2017) 033, arXiv:1704.04104 [hep-ex].
70. V. Lubicz *et al.*, PoS LATTICE2016 (2016) 290, arXiv:1610.09668 [hep-lat].
71. V. Cirigliano and H. Neufeld, Phys. Lett. B700 (2011) 7–10, arXiv:1102.0563 [hep-ph].
72. J. L. Rosner, S. Stone, and R. S. Van de Water, *Submitted to Particle Data Book*, arXiv:1509.02220 [hep-ph].
73. M. Antonelli *et al.* (FlaviaNet Working Group on Kaon Decays), Eur. Phys. J. C69 (2010) 399–424, arXiv:1005.2323 [hep-ph].
74. N. Carrasco *et al.*, Phys. Rev. D91 (2015) 074506, arXiv:1502.00257 [hep-lat].
75. L. Lellouch and M. Lüscher, Commun. Math. Phys. 219 (2001) 31–44, arXiv:hep-lat/0003023.
76. T. Blum *et al.* (RBC/UKQCD Collaboration), Phys. Rev. D91 (2015) 074502, arXiv:1502.00263 [hep-lat].
77. Z. Bai *et al.* (RBC/UKQCD Collaboration), Phys. Rev. Lett. 115 (2015) 212001, arXiv:1505.07863 [hep-lat].
78. N. Ishizuka, K. I. Ishikawa, A. Ukawa, and T. Yoshié, Phys. Rev. D92 (2015) 074503, arXiv:1505.05289 [hep-lat].
79. A. Alavi-Harati *et al.* (KTeV Collaboration), Phys. Rev. D67 (2003) 012005, arXiv:hep-ex/0208007.
80. J. R. Batley *et al.* (NA48 Collaboration), Phys. Lett. B544 (2002) 97–112, arXiv:hep-ex/0208009.
81. E. Abouzaid *et al.* (KTeV Collaboration), Phys. Rev. D83 (2011) 092001,

- arXiv:1011.0127 [hep-ex].
82. A. J. Buras, M. Gorbahn, S. Jäger, and M. Jamin, JHEP 11 (2015) 202, arXiv:1507.06345 [hep-ph].
 83. T. Kitahara, U. Nierste, and P. Tremper, JHEP 12 (2016) 078, arXiv:1607.06727 [hep-ph].
 84. C. Kelly, EPJ Web Conf. 175 (2018) 13020.
 85. C. Kelly, PoS LATTICE2016 (2016) 308.
 86. N. H. Christ, X. Feng, A. Jüttner, A. Lawson, A. Portelli, and C. T. Sachrajda (RBC/UKQCD Collaboration), Phys. Rev. D94 (2016) 114516, arXiv:1608.07585 [hep-lat].
 87. Z. Bai, N. H. Christ, X. Feng, A. Lawson, A. Portelli, and C. T. Sachrajda (RBC/UKQCD Collaboration), Phys. Rev. Lett. 118 (2017) 252001, arXiv:1701.02858 [hep-lat].
 88. Y. Amhis *et al.* (Heavy Flavor Averaging Group), Eur. Phys. J. C77 (2017) 895, arXiv:1612.07233 [hep-ex].
 89. C.-H. Chen and S.-h. Nam, Phys. Lett. B666 (2008) 462–466, arXiv:0807.0896 [hep-ph].
 90. E. Gulez, A. Gray, M. Wingate, C. T. H. Davies, G. P. Lepage, and J. Shigemitsu (HPQCD Collaboration), Phys. Rev. D73 (2006) 074502, arXiv:hep-lat/0601021.
 91. J. M. Flynn, T. Izubuchi, T. Kawanai, C. Lehner, A. Soni, R. S. Van de Water, and O. Witzel (RBC/UKQCD Collaboration), Phys. Rev. D91 (2015) 074510, arXiv:1501.05373 [hep-lat].
 92. J. A. Bailey *et al.* (Fermilab/MILC Collaboration), Phys. Rev. D92 (2015) 014024, arXiv:1503.07839 [hep-lat].
 93. J. A. Bailey *et al.* (Fermilab/MILC Collaboration), Phys. Rev. D92 (2015) 034506, arXiv:1503.07237 [hep-lat].
 94. H. Na, C. M. Bouchard, G. P. Lepage, C. Monahan, and J. Shigemitsu (HPQCD Collaboration), Phys. Rev. D92 (2015) 054510, arXiv:1505.03925 [hep-lat].
 95. P. del Amo Sanchez *et al.* (BaBar Collaboration), Phys. Rev. D83 (2011) 032007, arXiv:1005.3288 [hep-ex].
 96. J. P. Lees *et al.* (BaBar Collaboration), Phys. Rev. D86 (2012) 092004, arXiv:1208.1253 [hep-ex].
 97. B. Aubert *et al.* (BaBar Collaboration), Phys. Rev. Lett. 104 (2010) 011802, arXiv:0904.4063 [hep-ex].
 98. H. Ha *et al.* (Belle Collaboration), Phys. Rev. D83 (2011) 071101, arXiv:1012.0090 [hep-ex].
 99. A. Sibidanov *et al.* (Belle Collaboration), Phys. Rev. D88 (2013) 032005, arXiv:1306.2781 [hep-ex].
 100. R. Glattauer *et al.* (Belle Collaboration), Phys. Rev. D93 (2016) 032006, arXiv:1510.03657 [hep-ex].
 101. C. Bourrely, B. Mochel, and E. de Rafael, Nucl. Phys. B189 (1981) 157–181.
 102. Z. Gelzer *et al.*, EPJ Web Conf. 175 (2018) 13024, arXiv:1710.09442 [hep-lat].
 103. B. Colquhoun, S. Hashimoto, and T. Kaneko (JLQCD Collaboration), EPJ Web Conf. 175 (2018) 13004, arXiv:1710.07094 [hep-lat].
 104. J. A. Bailey *et al.* (Fermilab/MILC Collaboration), Phys. Rev. D89 (2014) 114504, arXiv:1403.0635 [hep-lat].
 105. I. Caprini, L. Lellouch, and M. Neubert, Nucl. Phys. B530 (1998) 153–181, arXiv:hep-ph/9712417.
 106. D. Bigi, P. Gambino, and S. Schacht, Phys. Lett. B769 (2017) 441–445, arXiv:1703.06124 [hep-ph].

107. B. Grinstein and A. Kobach, *Phys. Lett.* B771 (2017) 359–364, arXiv:1703.08170 [hep-ph].
108. F. U. Bernlochner, Z. Ligeti, M. Papucci, and D. J. Robinson, *Phys. Rev.* D96 (2017) 091503, arXiv:1708.07134 [hep-ph].
109. A. Vaquero Avilés-Casco *et al.*, *EPJ Web Conf.* 175 (2018) 13003, arXiv:1710.09817 [hep-lat].
110. C. J. Monahan, H. Na, C. M. Bouchard, G. P. Lepage, and J. Shigemitsu (HPQCD Collaboration), *Phys. Rev.* D95 (2017) 114506, arXiv:1703.09728 [hep-lat].
111. C. M. Bouchard, G. P. Lepage, C. Monahan, H. Na, and J. Shigemitsu (HPQCD Collaboration), *Phys. Rev.* D90 (2014) 054506, arXiv:1406.2279 [hep-lat].
112. F. Bahr, D. Banerjee, F. Bernardoni, A. Joseph, M. Koren, H. Simma, and R. Sommer (ALPHA Collaboration), *Phys. Lett.* B757 (2016) 473–479, arXiv:1601.04277 [hep-lat].
113. J. A. Bailey *et al.* (Fermilab/MILC Collaboration), *Phys. Rev.* D85 (2012) 114502, arXiv:1202.6346 [hep-lat].
114. M. Atoui, V. Morénas, D. Bečirević, and F. Sanfilippo, *Eur. Phys. J.* C74 (2014) 2861, arXiv:1310.5238 [hep-lat].
115. W. Detmold, C. Lehner, and S. Meinel, *Phys. Rev.* D92 (2015) 034503, arXiv:1503.01421 [hep-lat].
116. S. Meinel, *Phys. Rev. Lett.* 118 (2017) 082001, arXiv:1611.09696 [hep-lat].
117. W. Detmold and S. Meinel, *Phys. Rev.* D93 (2016) 074501, arXiv:1602.01399 [hep-lat].
118. R. Aaij *et al.* (LHCb Collaboration), *JHEP* 06 (2015) 115, arXiv:1503.07138 [hep-ex].
119. S. Descotes-Genon, J. Matias, and J. Virto, *Phys. Rev.* D88 (2013) 074002, arXiv:1307.5683 [hep-ph].
120. A. Bazavov *et al.* (Fermilab/MILC Collaboration), *Phys. Rev.* D93 (2016) 113016, arXiv:1602.03560 [hep-lat].
121. G. P. Lepage and P. B. Mackenzie, *Phys. Rev.* D48 (1993) 2250–2264, arXiv:hep-lat/9209022.
122. N. Carrasco *et al.* (ETM Collaboration), *JHEP* 03 (2014) 016, arXiv:1308.1851 [hep-lat].
123. A. V. Manohar and M. B. Wise, *Phys. Rev.* D49 (1994) 1310–1329, arXiv:hep-ph/9308246.
124. K. Maltman, R. Hudspith, R. Lewis, T. Izubuchi, H. Ohki, and J. Zanotti, *PoS CKM2016* (2017) 030.
125. S. Hashimoto, *PTEP* 2017 (2017) 053B03, arXiv:1703.01881 [hep-lat].
126. K.-F. Liu, *Phys. Rev.* D96 (2017) 033001, arXiv:1703.04690 [hep-ph].
127. M. T. Hansen, H. B. Meyer, and D. Robaina, *Phys. Rev.* D96 (2017) 094513, arXiv:1704.08993 [hep-lat].
128. P. Boyle *et al.*, *EPJ Web Conf.* 175 (2018) 13011.
129. P. Boyle *et al.* (RBC/UKQCD Collaboration), arXiv:1803.07228 [hep-lat].
130. S. Hashimoto, B. Colquhoun, T. Izubuchi, T. Kaneko, and H. Ohki, *EPJ Web Conf.* 175 (2018) 13006.
131. K. Hagiwara, R. Liao, A. D. Martin, D. Nomura, and T. Teubner, *J. Phys.* G38 (2011) 085003, arXiv:1105.3149 [hep-ph].
132. F. Jegerlehner, *EPJ Web Conf.* 166 (2018) 00022, arXiv:1705.00263 [hep-ph].
133. M. Davier, A. Hoecker, B. Malaescu, and Z. Zhang, *Eur. Phys. J.* C77 (2017) 827, arXiv:1706.09436 [hep-ph].
134. G. W. Bennett *et al.* (Muon g-2 Collaboration), *Phys. Rev.* D73 (2006) 072003,

- arXiv:hep-ex/0602035.
135. J. Grange *et al.* (Muon g-2 Collaboration), arXiv:1501.06858 [physics.ins-det].
 136. M. Otani (E34 Collaboration), JPS Conf. Proc. 8 (2015) 025008.
 137. G. Colangelo, M. Hoferichter, M. Procura, and P. Stoffer, JHEP 09 (2014) 091, arXiv:1402.7081 [hep-ph].
 138. V. Pauk and M. Vanderhaeghen, arXiv:1403.7503 [hep-ph].
 139. G. Colangelo, M. Hoferichter, M. Procura, and P. Stoffer, Phys. Rev. Lett. 118 (2017) 232001, arXiv:1701.06554 [hep-ph].
 140. J. Bijnens, E. Pallante, and J. Prades, Nucl. Phys. B474 (1996) 379–420, arXiv:hep-ph/9511388.
 141. M. Hayakawa, T. Kinoshita, and A. I. Sanda, Phys. Rev. Lett. 75 (1995) 790–793, arXiv:hep-ph/9503463.
 142. K. Melnikov and A. Vainshtein, Phys. Rev. D70 (2004) 113006, arXiv:hep-ph/0312226.
 143. B. E. Lautrup and E. De Rafael, Phys. Rev. 174 (1968) 1835–1842.
 144. T. Blum, Phys. Rev. Lett. 91 (2003) 052001, arXiv:hep-lat/0212018.
 145. M. Göckeler, R. Horsley, W. Kurzinger, D. Pleiter, P. E. L. Rakow, and G. Schierholz (QCDSF Collaboration), Nucl. Phys. B688 (2004) 135–164, arXiv:hep-lat/0312032.
 146. C. Aubin and T. Blum, Phys. Rev. D75 (2007) 114502, arXiv:hep-lat/0608011.
 147. X. Feng, K. Jansen, M. Petschlies, and D. B. Renner (ETM Collaboration), Phys. Rev. Lett. 107 (2011) 081802, arXiv:1103.4818 [hep-lat].
 148. D. Bernecker and H. B. Meyer, Eur. Phys. J. A47 (2011) 148, arXiv:1107.4388 [hep-lat].
 149. X. Feng, S. Hashimoto, G. Hotzel, K. Jansen, M. Petschlies, and D. B. Renner, Phys. Rev. D88 (2013) 034505, arXiv:1305.5878 [hep-lat].
 150. A. Francis, B. Jaeger, H. B. Meyer, and H. Wittig, Phys. Rev. D88 (2013) 054502, arXiv:1306.2532 [hep-lat].
 151. M. Della Morte *et al.*, JHEP 10 (2017) 020, arXiv:1705.01775 [hep-lat].
 152. S. Borsanyi *et al.* (BMW Collaboration), arXiv:1711.04980 [hep-lat].
 153. T. Blum *et al.* (RBC/UKQCD Collaboration), arXiv:1801.07224 [hep-lat].
 154. B. Chakraborty, C. T. H. Davies, G. C. Donald, R. J. Dowdall, J. Koponen, G. P. Lepage, and T. Teubner (HPQCD Collaboration), Phys. Rev. D89 (2014) 114501, arXiv:1403.1778 [hep-lat].
 155. B. Chakraborty, C. T. H. Davies, J. Koponen, G. P. Lepage, M. J. Peardon, and S. M. Ryan, Phys. Rev. D93 (2016) 074509, arXiv:1512.03270 [hep-lat].
 156. B. Chakraborty, C. T. H. Davies, P. G. de Oliveira, J. Koponen, G. P. Lepage, and R. S. Van de Water (HPQCD Collaboration), Phys. Rev. D96 (2017) 034516, arXiv:1601.03071 [hep-lat].
 157. F. Burger, X. Feng, G. Hotzel, K. Jansen, M. Petschlies, and D. B. Renner (ETM Collaboration), JHEP 02 (2014) 099, arXiv:1308.4327 [hep-lat].
 158. B. Chakraborty *et al.* (Fermilab/HPQCD/MILC Collaboration), arXiv:1710.11212 [hep-lat].
 159. D. Giusti, V. Lubicz, G. Martinelli, F. Sanfilippo, and S. Simula (ETM Collaboration), JHEP 10 (2017) 157, arXiv:1707.03019 [hep-lat].
 160. T. Blum *et al.* (RBC/UKQCD Collaboration), Phys. Rev. Lett. 116 (2016) 232002, arXiv:1512.09054 [hep-lat].
 161. T. Blum *et al.* (RBC/UKQCD Collaboration), JHEP 04 (2016) 063, arXiv:1602.01767 [hep-lat].
 162. B. Colquhoun, R. J. Dowdall, C. T. H. Davies, K. Hornbostel, and G. P. Lepage

- (HPQCD Collaboration), Phys. Rev. D91 (2015) 074514, arXiv:1408.5768 [hep-lat].
163. C. Aubin, T. Blum, M. Golterman, and S. Peris, Phys. Rev. D86 (2012) 054509, arXiv:1205.3695 [hep-lat].
 164. M. Golterman, K. Maltman, and S. Peris, Nucl. Part. Phys. Proc. 273-275 (2016) 1650–1656, arXiv:1410.8405 [hep-lat].
 165. S. Borsanyi *et al.*, Phys. Rev. D96 (2017) 074507, arXiv:1612.02364 [hep-lat].
 166. T. Izubuchi, Y. Kuramashi, C. Lehner, and E. Shintani, EPJ Web Conf. 175 (2018) 06020.
 167. T. Blum, N. Christ, M. Hayakawa, T. Izubuchi, L. Jin, C. Jung, and C. Lehner, Phys. Rev. Lett. 118 (2017) 022005, arXiv:1610.04603 [hep-lat].
 168. T. Blum, N. Christ, M. Hayakawa, T. Izubuchi, L. Jin, and C. Lehner, Phys. Rev. D93 (2016) 014503, arXiv:1510.07100 [hep-lat].
 169. A. Gérardin, H. B. Meyer, and A. Nyffeler, Phys. Rev. D94 (2016) 074507, arXiv:1607.08174 [hep-lat].
 170. T. Blum, N. Christ, M. Hayakawa, T. Izubuchi, L. Jin, C. Jung, and C. Lehner, Phys. Rev. D96 (2017) 034515, arXiv:1705.01067 [hep-lat].